EUROPEAN ORGANIZATION FOR NUCLEAR RESEARCH
European Laboratory for Particle Physics

Large Hadron Collider Project

LHC Project Report 801

The Effect of CuSn Intermetallics on the Interstrand Contact Resistance in Superconducting Cables for the Large Hadron Collider (LHC)

Ph. Gasser[1], P. Jacob[1] , D. Leroy[2], L. Oberli[2], C. Scheuerlein[2], M. Taborelli[2]

Abstract

The LHC superconducting cables are submitted to a 200°C heat-treatment in air in order to increase the resistance between the crossing strands (R_C) within the cable. During this treatment the as-applied Sn-Ag alloy strand coating is transformed into a CuSn intermetallic compound layer. The microstructure, the surface topography and the surface chemistry of the non-reacted and reacted coatings have been characterised by different techniques, notably focused ion beam (FIB), transmission electron microscopy (TEM), energy dispersive X-ray spectroscopy (EDS) and X-ray photoelectron spectroscopy (XPS). Based on the results obtained by these techniques the different influences that the intermetallics have on R_C are discussed.

The desired R_C is obtained only when a continuous Cu_3Sn layer is formed, i.e. a sufficient wetting of the Cu substrate by the tinning alloy is crucial. Among other effects the formation of the comparatively hard intermetallics roughens the surface and, thus, reduces the true contact area and it strongly affects the oxide growth on the strand surface. The oxide formed on the fully reacted coatings, which may contain essentially Cu-oxides, appears to be more stable, both mechanically and thermally, as compared to the oxide formed on the tinning alloy.

1 EMPA, Dübendorf, Switzerland
2 CERN, Accelerator Technology Departement & Technical Support Department, Geneva, Switzerland

To be published in Journal of Applied Physics

CERN
CH - 1211 Geneva 23
Switzerland

Geneva, 2 December 2004

I. Introduction

For the construction of the superconducting (SC) magnets of the Large Hadron Collider (LHC) [1], CERN's next particle collider, about 7000 km of Rutherford superconducting cables, composed of either 28 or 36 strands, are needed [2].

In order to reduce coupling currents between the strands and at the same time allow sufficient current sharing for the superconductor stability, the contact resistance of the crossing strands in the cables (interstrand contact resistance R_C) in the LHC magnets at 1.9 K should be between 20 and 100 μΩ. For this purpose a Sn-Ag coating is applied onto the copper matrix of the strands, which is subsequently submitted to a 200 °C heat-treatment in air, lasting typically a few hours. The Sn-Ag coating is applied by a continuous hot-dip process [3,4,5].

The desired resistance between the crossing strands is obtained only after the cable heat-treatment, which causes, among other effects, the interdiffusion of Sn and Cu and the formation of intermetallic phases, the modification and part removal of surface contaminants and the growth of the surface oxides. Several researchers have studied the interstrand contact resistance in cables with different strand surfaces [6,7] and the contact resistance of heat-treated Sn-Ag coatings in particular [8]. For most heat-treated strand types it is concluded that it is the surface oxide that determines R_C.

Since the development of the LHC strand coating the intermetallics in Cu-Sn interdiffusion pairs have attracted much attention, for instance in view of the development of lead free solders [9] and advanced joining techniques for electronic packaging and microelectronics applications (see for instance reference 10). In solder joints an intermetallic layer is generally present between solder and the metal to be soldered, forming the required structural bond between both materials [11]. During prolonged storage or during heat-treatments (solder reflow) the intermetallics grow, which is detrimental to the joint since intermetallics can reduce the wetability of pre-tinned substrates [12] and they can degrade the mechanical properties of the joint [13].

When Sn containing solders are used in combination with Cu the intermetallic compounds that are formed are Cu_6Sn_5 (η-phase) and Cu_3Sn (ε-phase) [14]. The compound that is initially formed during liquid-solid reactions is Cu_6Sn_5, which grows initially much faster than Cu_3Sn. Once all Sn is changed into Cu_6Sn_5 the Cu_3Sn phase continues to grow at the expense of Cu_6Sn_5, forming small grain sized planar layers. A commonly used lead free solder is the eutectic Sn-3.5Ag alloy. For Sn-3.5Ag/Cu couples at 170 °C and at 205 °C a $t^{0.42}$ time dependence has been found for the Cu_3Sn growth [15]. The kinetics for the intermetallic formation and the intermetallic microstructure depend for instance on the cooling rate [16] and the presence of other elements in the coating bath, such as Cu [17], which is dissolved in the coating bath from the strand during the coating process.

In the Sn-3.5Ag solder Ag is present in the form of Ag_3Sn particles, which are more or less finely dispersed, depending on the cooling rate. The presence of the Ag_3Sn particles slightly increases the solder strength as compared to pure Sn and they may prevent the formation of Sn whiskers as it is observed on thin Sn films on Cu substrates [18]. At

temperatures below 170 °C the Ag content reduces the growth of CuSn intermetallics as compared to the intermetallics growth in interdiffusion couples of pure Sn and Cu, while a similar growth rate is reported at 205 °C [15]. As in the case of the pure Cu matrix Ag is not dissolved in the CuSn intermetallic layer but it can be incorporated in the form of Ag_3Sn.

Like ceramics the covalently bonded intermetallic compounds are hard and brittle. Unlike ceramics and similarly to metals, intermetallics conduct electricity and heat rather well. In Table I some materials properties found in literature for Cu_3Sn and Cu_6Sn_5 bulk are compared with those for Cu, Sn and the eutectic Sn-3.5Ag (wt.%) alloy. Despite the fact that the hardness values shown are difficult to compare because of the different measurement methods and parameters used, it is clear that the intermetallics are significantly harder than Cu, Sn and their alloys.

In the present article the influence of the CuSn intermetallics on the contact resistance in LHC superconducting cables is assessed on the basis of experimental results that have been obtained by Focused Ion Beam (FIB) analysis, a technique that has now become accessible for the characterisation of surface coatings and oxide layers [19]. FIB was used in combination with a Transmission Electron Microscope (TEM) and Energy Dispersive X-ray Spectroscopy (EDS). The types of oxides present on the strand surface have been determined by X-ray Photoelectron Spectroscopy (XPS).

II. Experimental

The strand samples

The samples that have been analysed are LHC superconducting strands taken from cables of different manufacturers. One strand coating was analysed in the as-applied state, i.e. without subsequent heat-treatment. All other samples followed a 200 °C treatment in air as it is applied to the LHC cables in order to obtain the required R_C. Before materials characterisation the cable samples were used for R_C measurements. The samples that were analysed by FIB are described in Table II. One sample (heat-treated 02B) exhibits a rather high contact resistance while the contact resistance of the three 02D samples is below the specified limits.

The average strand coating thickness given in Table II is calculated from the Sn coating mass, which is routinely determined by wet chemistry methods, notably amperostatic coulometry [20] and atomic absorption spectroscopy. The average Ag content in the strand coating is typically about 3.3 at.% [21], i.e. somewhat below the eutectic composition of the Sn-Ag system, which is 3.8 at.% (3.5 wt.%) Ag [14], and significantly below the nominal Ag content in the strand coating bath, which is 5.5 at.% Ag (5 wt.% of Ag). An analysis of coating bath samples obtained from different strand manufacturers shows that the bath contains also typically between 1 and 4 at.% of Cu in addition to Sn and Ag.

Optical metallography on different strand samples shows that the coating thickness along the circumference of one strand may vary by more than one order of magnitude, with thickness values ranging from a tenth of a µm to several µm. The important thickness variations that are observed by optical metallography have been confirmed by other

methods, for instance by X-ray fluorescence (XRF) thickness measurements [20]. The coatings on heat-treated strands are found to be significantly thicker than the as-applied coatings. Since the densities of Cu_6Sn_5 and Cu_3Sn are 8.28 and 8.90 g cm^{-3} [32], similar to the densities of Cu (8.94 g cm^{-3}) and Sn (7.28 g cm^{-3}), one can expect an approximately four fold thickness increase when the entire Sn transforms into Cu_3Sn.

Focused Ion Beam

FIB is a technique that allows a mechanically stress-free microcleaving by means of a gallium ion beam. The equipment setup is comparable to a scanning electron microscope, where the electron gun has been replaced or supplemented by a gallium ion beam (see Figure 1). This technique has originally been developed for semiconductor device characterization and microstructure device modifications: by using additional process gases, both material-selective milling and depositions of certain metals and oxides are possible, too.

The ion beam allows both milling by ion sputtering and imaging by secondary electrons or secondary ions. The contrast signal, however, gives some more information than that of an electron microscope, since the penetration depth of the primary ions strongly depends on crystal orientation (ion channelling), so that grains become clearly visible. The cross sections shown in this article demonstrate this effect clearly. Neither previous chemical decoration or other pre-treatment is necessary for this, nor any change to another instrument: the inspection can be performed directly in the tool, by just tilting the sample to 45 degrees to inspect the cross-section.

The resolution of FIB is about 10 nm. Even at low-current primary beam (less than 30 pA), slight sputtering of material will take place. Normally, this is not critical; however, when preparing very thin TEM-lamellas (less than 100 nm) or surface imaging of ultrathin layers, the effect might not be negligible. To cover those applications, too, many FIBs are equipped with an additional electron beam column (so-called “dual-beam”-FIBs). This allows in-situ SEM inspections of the ion milling/polishing progress and final inspections of TEM lamellas. Since ion gun and electron gun are mechanically mounted at an angle of 45-52 degrees, SEM-inspection of the FIB-milled cross section does not need any tilting of the sample. This is very advantageous in the case of precisely prepositioned samples.

TEM sample preparation by focused ion beam milling and TEM analysis

When an extremely high resolution is needed, an investigation by means of transmission electron microscopy is necessary. This needs the preparation of a thin, electron-transparent film sample of less than 100 nm thickness. FIB is an ideal tool to perform such preparation [22]. In principle, a cross section is made first from one side, followed by another cross section of exactly the same dimensions from the other side. The remaining thin TEM lamella can be cut out by FIB, too. Finally, the lamella is transferred by a glass needle to a TEM grid for further analysis. Samples for TEM investigation had been prepared with a FEI Strata DB 235 dual-beam (DB) FIB workstation. The DB workstation incorporates a FIB and a SEM column tilted with respect to each other by an angle of 52°.

The SEM Column is equipped with a FEG emitter and an in-lens detector. Resolution is specified to be 3 nm at 1 kV. The FIB Column is adjustable from 1 pA to 20 nA at 30 kV with a specified resolution of 7 nm, as given by the manufacturer. The instrument is equipped with four secondary electron and ion detectors. The Workstation has a digital patterning generator and four gas injection systems for deposition and specific etching processes.

The TEM specimens were prepared by milling an electron-transparent sample (e.g. 20 µm long, 5 µm wide and 100 nm thick) out of a bulk metallographic sample. The TEM lamellas were transferred onto carbon coated TEM grids (Ni) using an optical microscope and a micromanipulator.

TEM images and EDS analysis were performed on a CM 30 Philips with LaB_6 source. The TEM was operated at 200 kV. Images were recorded with a Gatan CCD model 694 in bright field mode. The EDS analysis was performed with an EDAX DX-4 equipped with a Li doped Si semi-conductor detector, Edax 139-10 with SUT window. For elemental analysis the TEM was operated in nanoprobe mode.

III. Results

Macroscopic appearance of the interstrand contact area in Rutherford-type LHC cables

In Figure 2 the strand deformation at the contact areas between the crossing strands inside the Rutherford-type cables can be seen. On a macroscopic scale it seems that the entire load bearing area has yielded plastically and is equal to the strand contact area.

FIB analysis of coating cross sections

The coating microstructure and the coating surface topography have been examined by FIB. In Figure 3 FIB cross sections through a non-heat-treated strand coating and its underlying copper matrix are shown. The FIB images reveal also the surface topography of the coating outside (left image) and inside the interstrand contact area (right image). The as-applied coating (left image) appears as clusters and not as a homogeneous film. During the cabling process the coating is smoothened inside the interstrand contact area (right image). The coating is too thin and irregular for a thickness measurement from the FIB images. The plastic strand deformation that occurs during cabling is also shown by grain size and shape variations that are caused by cold working of the Cu matrix.

The FIB images shown in Figure 4 have been acquired on a heat-treated strand from a cable for which comparatively high R_C values have been measured (the strand was produced by the same manufacturer as the one shown in Figure 3). The coating outside the contact zone (left image) is somewhat thicker than the adjacent coating inside the interstrand contact area. The rather rough surface topography appears to be similar in both cases, i.e. contrary to what is observed on the non heat-treated strand, inside the contact zone the coating is not smoother than it is outside the contact zone.

In Figure 5 the FIB cross section of a strand coating that was reacted for 8 h (left image) is compared with that of a strand that was heated to 200 °C for 3 h only. While after 8 h the coating is fully reacted, the upper part of the coating that was only heated during 3

hours is not fully reacted. The surface of the fully reacted coating is much rougher than the surface of the coating which is only partly reacted.

Both FIB cuts in Figure 5 have been obtained outside the contact area. As for all other strands that were examined the adjacent coating inside the compressed contact zone is significantly thinned.

TEM analysis of the intermetallic layer and surface oxides

Lamellas produced by FIB were analysed in a TEM in order to examine the intermetallic layer in more detail and to estimate the thickness of the strand oxide after thermal treatment. In Figure 6 the strand coating cross section obtained for the heat-treated cables 02B and 02D-b are shown.

On the 02B sample a homogeneous small grain sized intermetallic coating with a thickness between 0.7 and 1 µm is seen. At the interface so-called Kirkendall voids are visible that are produced during the Cu and Sn interdiffusion process. An EDS analysis at different points in the intermetallic layer gives a constant Sn concentration across the layer. A precise quantitative result cannot be given because no standard sample was available but EDS indicates that the layer is composed of Cu_3Sn rather then Cu_6Sn_5.

The FIB cross section of the 02D-b sample shows that on this sample the intermetallic layer is very irregular and locally even absent. Instead of the columnar grain shape on the 02B sample grains appear to be rather round on the 02D strands. The appearance of the other 02D samples (02D-a and 02D-c) is also similar to that of the 02D-b sample.

A TEM analysis of the FIB cross sections allows the oxide thickness on the outer strand surface to be estimated. In Figure 7 the oxide layer on the 02B and the 02D sample is shown. The oxide layer is embedded between the intermetallic layer and a protective Pt layer.

From Figure 7 the oxide thickness that is present on the strand coating after the thermal treatment (9.4 h at 200 °C in air) can be estimated as about 30 nm. The oxide layers on all 02D strands that were examined are irregular with thicknesses on some locations not exceeding those of native oxides as they are formed at room temperature (about 3 nm).

Surface oxides as determined by XPS

From the peak positions and shape in the high resolution photoelectron spectra (see example in Figure 8) it can be seen that the oxides on the outermost heat-treated strand surfaces contain CuO and either SnO or SnO_2 (SnO and SnO_2 cannot be easily distinguished by XPS).

The proportion of Cu and Sn oxide varies strongly for different strands within one cable and also for different cable types. For cable 02B and 02D-b the ratio Cu to Sn has been determined semi-quantitatively for all strands (one analysis in the contact zone of each strand) and it was found that in average the 02B strand surfaces are richer in Cu-oxides than the 02D strands.

IV. Discussion

The bulk resistance of the Cu matrix in Cu-stabilised strands has a negligibly small influence on R_C [8]. Hence, the outer strand surface layer plays a dominant role on R_C.

The coating cross section images obtained by FIB and TEM show that during the 200 °C cable heat-treatment the as-applied coating is transformed into an intermetallic layer composed of small grains. EDS analysis indicates that when the entire Sn has reacted, mainly Cu_3Sn is present in the coating, which is in agreement with the results presented for instance in references 15 and 23.

The intermetallic layer may affect R_C through its bulk resistivity, its surface topography and through its influence on the surface oxides that are formed during the cable heat-treatment in air. The contribution of each of these parameters on R_C is discussed below.

The influence of the intermetallic bulk resistivity and coating thickness on R_C

It can be shown that for a certain cable type there is a trend of R_C to decrease with increasing coating thickness under identical heat-treatment conditions. Therefore, heat-treatment times are adapted, i.e. the thicker the average Sn-Ag coating in a cable the longer is the heat-treatment time that is needed to get the desired R_C values. The fact that there is a trend of R_C to decrease with increasing coating thickness is a clear indication that R_C is not mainly determined by the intermetallic bulk resistivity. This is also confirmed by the resisitivity values shown in Table I for Cu_3Sn and Cu_6Sn_5, which are both similar to the Sn-3.5Ag solder alloy electrical resistivity.

Variations of the true interstrand contact area during thermal treatment

The strands in Rutherford cables may be described as cylinders that are placed cross wise (so-called cross rod contacts). During the cabling process and in the magnet coils the strand contacts yield under the applied contact load, forming the interstrand contact areas that are seen in Figure 2 on a macroscopic scale. As shown in the FIB images in Figure 3 both the Cu strand matrix and the soft Sn-Ag coating alloy yield plastically during the cabling process.

During the 200 °C cable heat-treatment the surface roughness is strongly increased with respect to the non heat-treated coating due to the entire transformation of the coating alloy into the hard Cu_3Sn intermetallic layer. A comparison between the FIB images acquired outside and inside the contact zone of the heat-treated strands (see Figure 4) indicates that there is hardly any plastic deformation of the comparatively hard Cu_3Sn layer under the average pressure of 50 MPa to which the LHC cable samples were exposed prior to the FIB analysis.

Because of the surface roughening and hardening it can be expected that the true contact area is reduced during the cable heat-treatment, provided that heat-treatment temperature and time are sufficient to react the entire Sn with Cu. The interstrand current flow is therefore restricted at the contact surface (constriction resistance). If the heat-treatment time is too short and a soft alloy layer remains this yields plastically under the applied

load, giving rise to a true contact area that can be even larger than that found on a non heat-treated strand (see Figure 5).

Apart from the contact topography the constriction resistance depends also on the conducting properties of the contact pair materials (metallic, semi-conducting or insulating). For the case of contacts between metallic conductors it can be shown that the contact resistance is nearly inversely proportional to the true contact area [24]. When, however, a metallic conductor is entirely covered by an insulating film through which electrons can penetrate through the tunnelling effect a reduction of the true contact area has a comparatively small influence on R_C [25].

As seen in Figure 6 the current flow between two strands is not only restricted at the outer strand surface but also at the Cu-Cu_3Sn interfaces. The restriction occurs at so-called Kirkendall voids, which are formed during the interdiffusion process in Cu-Sn pairs [26].

Influence of CuSn intermetallics on the surface oxidation

The formation of CuSn intermetallics can indirectly affect R_C by influencing the type and thickness of the surface oxides that grow during the cable heat-treatment in air.

The oxides present on pure Sn or Sn-3.5Ag oxidised in air at ambient conditions are supposed to be a mixture between SnO and SnO_2 [27]. However, despite the fact that the formation of Sn oxides is thermodynamically favoured over the formation of Cu oxides on heat-treated Cu_3Sn mainly Cu oxides have been detected (on Cu_6Sn_5 mainly Sn oxides are formed) [12]. The surface analysis results obtained at CERN confirm the presence of CuO on the heat-treated strands.

A particularly rapid oxide growth in air and in an oxygenated electrolyte is reported to occur on Cu_3Sn [27]. These oxides are more difficult to remove than the native oxides on the respective pure metals, which is a reason for the extreme difficulties to wet Cu_3Sn by Sn base solders. It is assumed that the oxides formed on Cu_3Sn, which can be composed essentially of Cu-oxides, mainly contribute to the contact resistance in the LHC cables.

The strand oxide films may be mechanically fractured when loaded. As seen in Figure 7 the oxides on the irregular intermetallic layers appear to be easily fractured, giving rise to the formation of metallic bridges through the oxide. These metal-to-metal contacts are likely to cause a significant R_C reduction as compared with the non-fractured oxide as it is observed on the 02B strand.

The formation of a continuous Cu_3Sn layer seems therefore to be required in order to obtain a homogeneous and sufficiently thick and stable strand oxide layer and, thus, to obtain the desired interstrand contact resistance in the LHC cables.

V. Conclusion

The intermetallic Cu_3Sn layer contributes to the contact resistance through an increased constriction resistance and through its influence on the oxides that are formed during the cable heat-treatment in air. The latter appears to be the more important effect. A more detailed study about the oxidation processes of the LHC superconducting strands will be addressed in a further study.

Acknowledgements

We are grateful to D. Richter for helpful advice about the LHC strand coatings and to G. Grossmann from the EMPA for fruitful discussions about CuSn intermetallics in solder joints.

Tables and Figures

Table I: Melting point, mechanical properties and electrical resistivity (at room temperature) of the strand coating materials found in literature. *The copper and tin hardness has been measured in metallographically prepared strand cross sections. **The hardness for the eutectoid Sn-3.5Ag (wt.%) alloy has been determined in a solder joint by nanoindentation using a Berkovitch indenter and an indent depth in the order of 100 nm. ***For Cu_3Sn, Cu_6Sn_5 and Ag_3Sn the hardness was measured on bulk samples with a Vickers indenter and a load of 10 N.

	Melting point [14]	Hardness	Young's modulus (GPa) [28]	Electrical resistivity (μΩ cm)
Cu	1080 °C	$HV_{0.5}$=80*	116.5	1.7 [29]
Sn	232 °C	HV0.005=15*	46.9	11.5
Sn-3.5Ag	220 °C	0.23 GPa **[30] (HV=23)	51.3	12.3 [9]
Cu_3Sn	676 °C	6.2 GPa ***[31] (HV=630)	134.2	8.8 [32]
Cu_6Sn_5	415 °C	6.5 GPa ***[31] (HV=660)	112.3	17.5 [32]
Ag_3Sn	480 °C	2.9 GPa ***[31] (HV=300)	78.9	

Table II: Heat-treatment time at 200 °C in air, interstrand contact resistance R_C (at LHC operating conditions) and average Sn coating thickness for all strands of the cables from which samples were analysed by FIB.

Cable type	Heat-treatment time (h)	R_C (μΩ)	Average pure Sn thickness of the cable (μm)
02B non heat-treated	0	Not measured	0.31
02B heat-treated	9.4	213	0.31
02D-a (heat-treated)	3	10	0.21
02D-b (heat-treated)	8	11	0.31
02D-c (heat-treated)	12	12	0.28

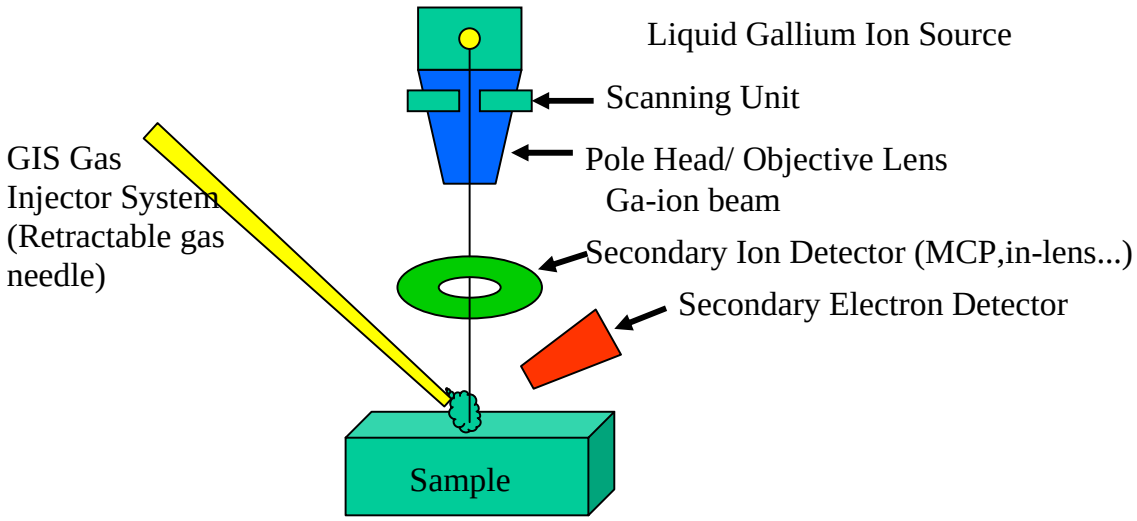

Figure 1: Principal FIB setup as it was used for strand coating characterisation.

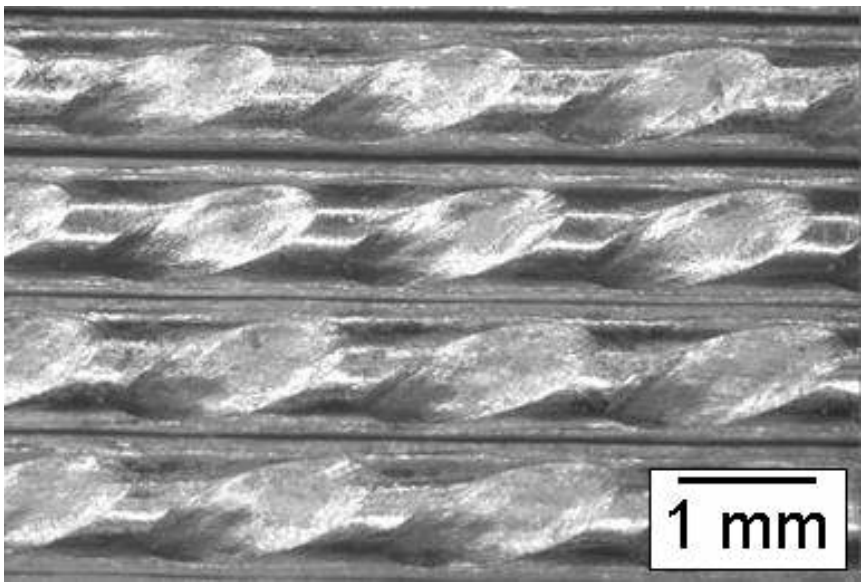

Figure 2: Light microscope image of four strands inside a (non-heat-treated) Rutherford type LHC cable. The interstrand contact areas are clearly visible. On a macroscopic scale the entire load bearing area seems to be plastically deformed.

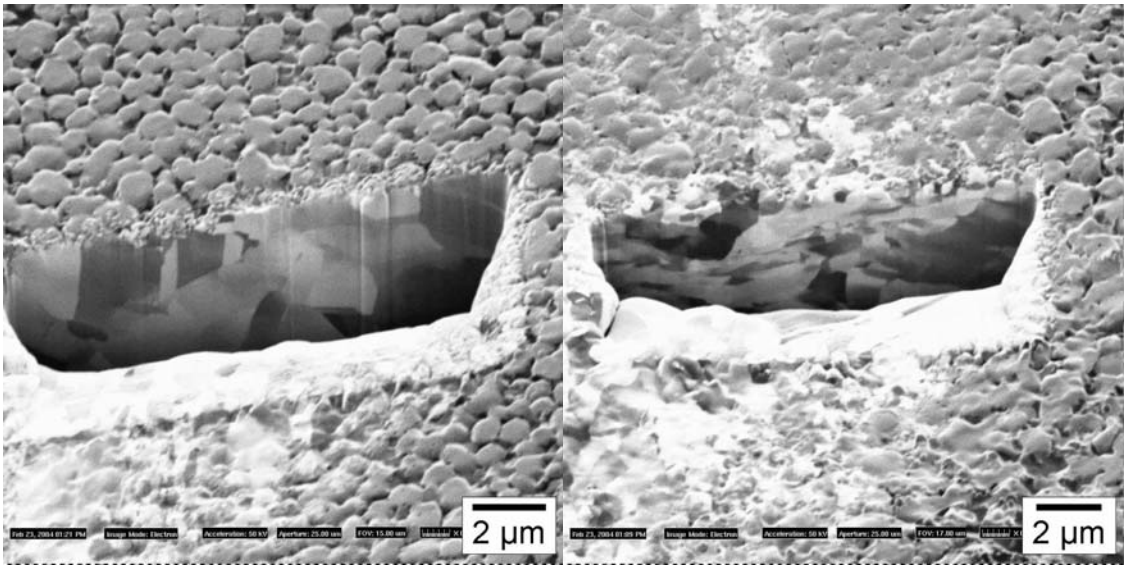

Figure 3: FIB image of a coating cross section on a strand taken from non heat-treated 02B cable. The left image represents the Sn-Ag coating outside and the right image inside the strand contact area. It can be seen that in the contact zone the coating surface yields plastically, thus increasing the true contact area. The strand deformation during cabling is also indicated by the Cu substrate grain size and shape changes that are revealed in the right FIB image.

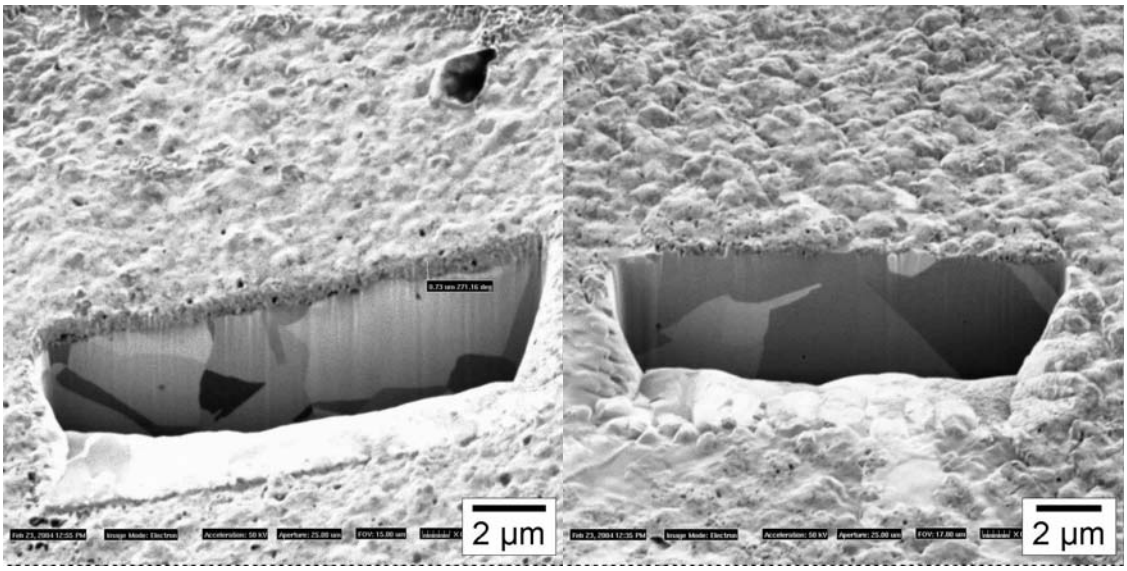

Figure 4: FIB strand coating cross sections for strand taken from heat-treated 02B cable outside (left image) and inside the interstrand contact area (right image). Both surfaces appear to be rougher than the as-applied coating.

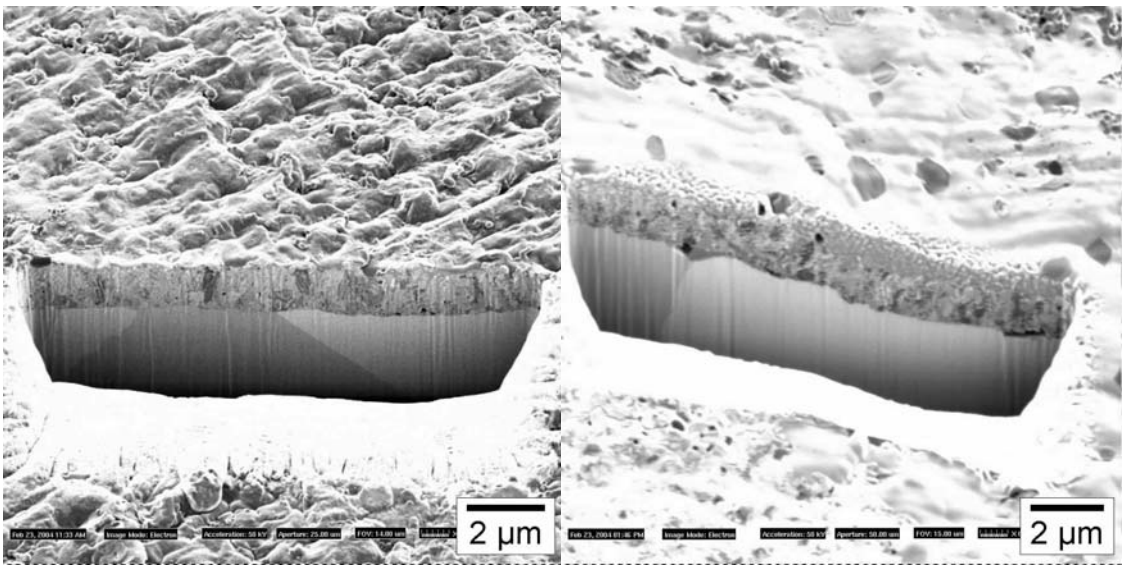

Figure 5: Strand coating cross sections produced by FIB for heat-treated strands taken from cable 02D-b after 8 h, 200 °C (left image) and 02D-a, after 3 h 200 °C (right image) outside contact area. After 3 h 200 °C heat-treatment the coating has not entirely reacted and a smooth alloy surface remains.

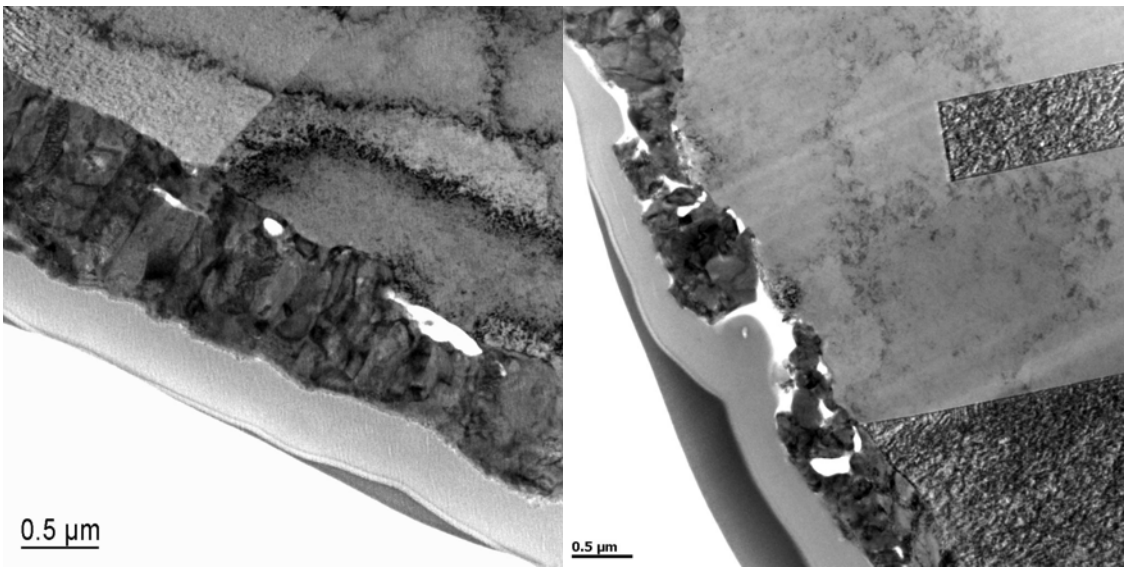

Figure 6: TEM image of the CuSn intermetallic layer of strand taken from heat-treated 02B cable (left image) and from 02D-b cable. On the 02B strand a homogenous Cu_3Sn layer composed of small grains with a thickness of approximately 0.7 to 1 µm is present. The bright areas at the CuSn intermetallic Cu interface are voids formed during the Cu-Sn interdiffusion process. The intermetallic layer on the 02D-b strand is irregular and locally even entirely absent.

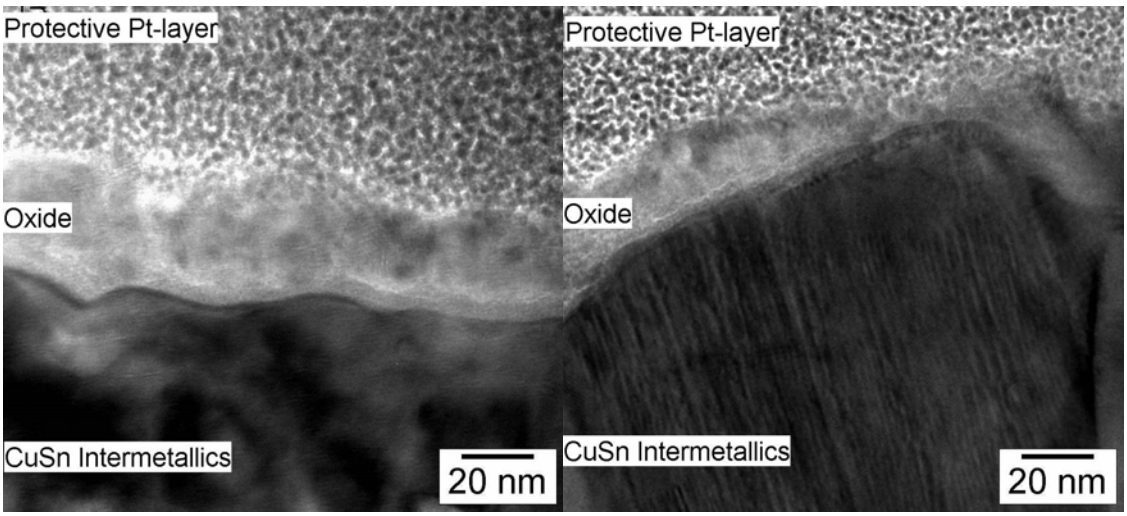

Figure 7: TEM image of FIB cross section that shows the strand oxide layer on the 02B (left image) and 02D-b sample (right image). On the 02B strand a continuous oxide layer with a thickness of approximately 30 nm is found (the oxide is embedded between the intermetallic layer and the protective Pt coating). The oxide layer on the 02D sample is irregular and locally its thickness is below the spatial resolution of the measurement method.

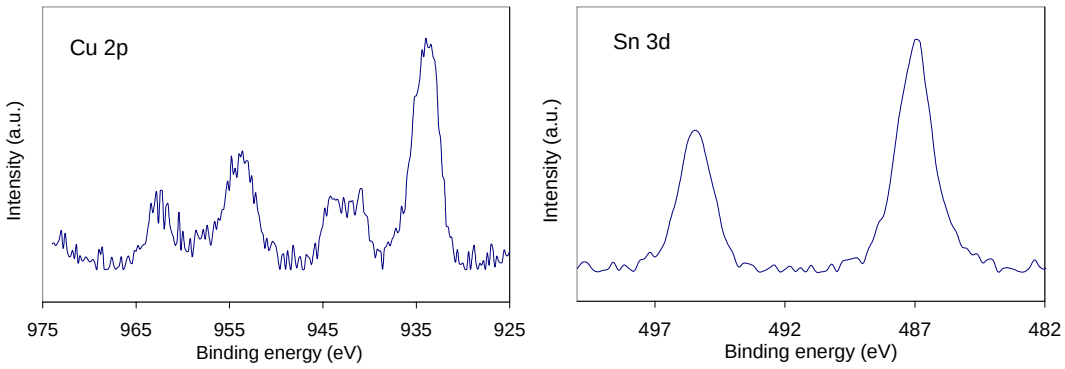

Figure 8: High resolution spectra of the Cu 2p and Sn 3p photoelectron peaks acquired on the 02D-a sample. Peak shape and positions indicate that the surface oxides are mainly CuO together with either SnO or SnO_2 (these two Sn oxides are difficult to distinguish from XPS data).

References

1 The LHC Study Group, "*The Large Hadron Collider, Conceptual Design*", CERN/AC/95-05, (1995)

2 J.D. Adam, T. Boutboul, G. Cavallari, Z. Charifoulline, C.H. Denarie, S. Le Naour, D.F. Leroy, L.R. Oberli, D. Richter, A.P. Verweij, R. Wolf, IEEE Trans. Appl. Supercond. 12(1), (2002), 1056

3 J.-M. Depond, D. Leroy, L.R. Oberli, D. Richter, IEEE Trans. Appl. Supercond, 7(2), (1997), 793

4 D. Richter, J.D. Adam, D. Leroy, L.R. Oberli, IEEE Trans. Appl. Supercond. 9(2), (1999), 735

5 D. Richter, J.D. Adam, J-M. Depond, D. Leroy, L.R. Oberli, IEEE Trans. Appl. Supercond., 7(2), (1997)

6 A.K. Ghosh, "*Interstrand Resistance Studies of Oxidized Superconducting Wires*", SSC Technical Note No. 103, SSCL-N-808, (1992)

7 A. Nijhuis, H.H.J. ten Kate, V. Pantsyrny, A.K. Shikov, M. Santini, IEEE Trans. Appl. Supercond. 10(1), (2000), 1051

8 M.D. Sumption, E.W. Collings, R.M. Scanlan, A. Nijhuis, H.H.J. ten Kate, S.W. Kim, M. Wake, T. Shintomi, Cryogenics 39(3), (1999)

9 B.R. Allenby et. all., Surface Mount Int. Vol. 2, (1992), 1251

10 P. Lauro, S.K. Kang, W.K. Choi, D.Y. Shi, J. Electron. Mat. 32(12), (2003), 1432

11 M.M. Schwartz, "*Fundamentals of Soldering*", in ASM Handbook Vol. 6, ASM International, (1993)

12 H.J. Reynolds, J.W. Morris, J. Electron. Mat., 24(10), (1995), 1429

13 W. Huang, J.M. Loman, B. Sener, Microelectronics Reliability 42, (2002), 1229

14 "*Alloy Phase Diagrams*", ASM Handbook Vol. 3, ASM International, (1992)

15 P.T. Vianco, K.L. Erickson, P.L. Hopkins, J. Electron. Mater.23(8), (1994), 721

16 F. Ochoa, JJ. Williams, N. Chawla, J. Electron. Mater. 32(12), (2003), 1414

17 I.E. Anderson, B.A. Cook, J. Harringa, R.L. Terpstra, J. Electron. Mater. 31(11), (2002), 1166

18 K.N. Tu, R.D. Thompson, Acta Metall. 30, (1982), 947

19 N. Presser, M.R. Hilton, Thin Solid Films, 308-309, (1997), 369

20 C. Scheuerlein, G. Arnau Izquierdo, N. Charras, L.R. Oberli, M. Taborelli, J. Electrochem. Soc. 151(6), (2004)

21 C. Scheuerlein, M. Carosone, S. Ilie, D. Letant, C. Petitjean, "*The measurement of the Ag concentration in the Sn-Ag hot dip coating of LHC superconducting strands*", CERN, AT-MAS Technical note 2004-01, (2004)

22 Ph. Gasser, U. Klotz, F.A. Khalid, O. Beffort, Microscopy & Microanalysis 10(2), (2004),1

23 S. Bader, W. Gust, H. Hieber, Acta Metall. Mater. 43(1), (1995), 329

24 L. Kogut, K. Komvopoulos, J. Appl. Phys. 94(5), (2003), 3153

25 L. Kogut, K. Komvopoulos, J. Appl. Phys. 95(2), (2004), 576

26 H. Oikawa, A. Hosoi, Scripta Metallurgica 9, (1975), 823

27 D.M. Tench, "*Oxidation of Solder Coatings*", in "*The Mechanics of Solder Alloy Wetting & Spreading*", edited by F.G. Yost, F.M. Hosking, D.R. Frear, Van Nostrand Reinhold, New York, (1993)

28 X. Deng, M. Koopman, N. Chawla, K.K. Chawla, Materials Science and Engineering A364, (2004), 240

29 Handbook of Chemistry and Physics, ed. D.R. Lide, 76th edition, CRC Press, (1995)

30 J.P. Lucas, A.W. Gibson, K.N. Subramanian, "Mat. Res. Soc. Symp. Proc. 522, (1998)

31 R.R. Chromik, R.P. Vinci, S.L. Allen, M.R. Notis, "J. Materials Research 18(9), (2003), 2251

32 H.P.R. Frederikse, R.J. Fields, A. Feldman, J. Appl. Phys. 72(7), (1992)